ACS OMEGA

Open Access

http://pubs.acs.org/journal/acsodf

Article

Hydrothermal Synthesis of a Magnesium Vanadate-Functionalized Reduced Graphene Oxide Nanocomposite for an Efficient Photocatalytic Hydrogen Production

Fahad A. Alharthi,* Adel El Marghany, Naaser A. Y. Abduh, and Imran Hasan*

Cite This: *ACS Omega* 2023, 8, 31493−31499

Read Online

ACCESS | Metrics & More | Article Recommendations | Supporting Information

ABSTRACT: Herein, we reported the fabrication of a magnesium vanadate-reduced graphene oxide ($Mg_3V_2O_8$-rGO) composite. Further, the structural morphology of the as-prepared $Mg_3V_2O_8$-rGO composite was studied by scanning electron microscopy. Powder X-ray diffraction and energy-dispersive X-ray spectroscopy techniques were also adopted to check the phase purity and elemental composition of the prepared $Mg_3V_2O_8$-rGO composite. $Mg_3V_2O_8$-rGO possesses a band gap of 2.98 eV, which prompted us to explore its photocatalytic activity for hydrogen (H_2) evolution reaction. The $Mg_3V_2O_8$-rGO composite demonstrated the generation of a reasonable amount of H_2 evolution (97.45 μmol g^{-1}), which is relatively higher than that of pristine $Mg_3V_2O_8$ (17.45 μmol g^{-1}). This may be attributed to the presence of synergism between $Mg_3V_2O_8$ and rGO. In addition, $Mg_3V_2O_8$-rGO also showed good stability and suggested its potential application for photocatalytic H_2 evolution applications. So far, no report is available on the use of $Mg_3V_2O_8$-rGO as a photocatalyst for H_2 evolution. We propose the potential role of the $Mg_3V_2O_8$-rGO composite for photocatalytic H_2 evolution applications.

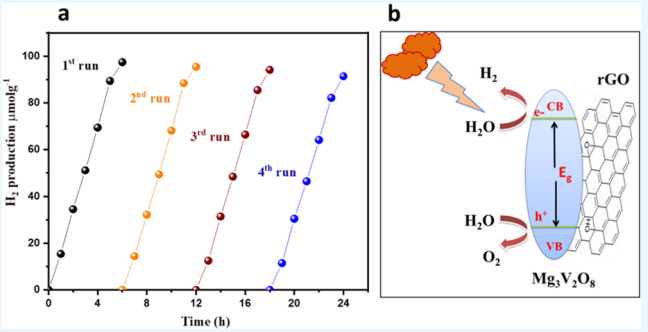

1. INTRODUCTION

In the past few years, a rapid surge in energy consumption has been observed.[1] This surge in energy consumption may be responsible for the energy crisis.[2] Currently, energy consumption relies on conventional energy resources such as coal, natural gas, waste, biomass, sun, wind, hydropower, nuclear power, and geothermal power.[3−5] However, these resources are limited and lead to increasing global warming-related issues.[6−9] Therefore, researchers have been attracted toward the design and development of energy-related devices and techniques such as solar cells, energy storage devices, batteries, and supercapacitors.[7]

Hydrogen (H_2) evolution or production has received enormous attention because of its eco-friendly nature and cost-effectiveness.[10,11] In particular, photocatalytic H_2 production has been considered the most efficient technique to produce H_2.[12] H_2 may be an alternative green energy source to overcome energy-related issues.[13] Therefore, it is of great importance to design or develop technologies for H_2 production. Fujishima et al.[14] reported the catalytic activities of titanium dioxide (TiO_2) for H_2 production applications. This review explores the potential applications of transition metal oxides/semiconducting metal oxides for H_2 production applications. The photocatalytic breakdown of water molecules into H_2 and oxygen requires semiconducting metal oxide-based photocatalyst.[15,16] In previous years, various photocatalysts such as tin oxide (SnO_2), nickel oxide (NiO), manganese oxide (MnO_2), graphitic carbon nitride (g-C_3N_4), copper oxide (CuO), cobalt oxide (Co_3O_4), perovskite-like materials, zinc oxide (ZnO), tungsten oxide (WO_3), etc. have been widely used for H_2 production applications.[17−24] However, many efficient photocatalysts have been reported for H_2 production but still there is a chance to further design and develop new photocatalysts for H_2 production applications.[23]

Recently, metal vanadate has received great interest from the scientific community because of its excellent chemical stability, electronic properties, narrow optical band gap, and cost-effectiveness.[25−32] In previous years, various metal vanadate materials, which include MVO_4, $M_2V_2O_7$, MV_2O_6, $M_3V_2O_8$, MV_2O_4, and MV_3O_8 (herein, M= Zn, Ni, Fe or Mn), have received significant attention of the researchers due to their reasonable optoelectronic properties and environment-friendly nature.[33−37] Particularly, $M_3V_2O_8$ has been extensively used as a suitable electrode material for various optoelectronic applications.[38] $Mg_3V_2O_8$ has various advantageous features

Received: June 23, 2023
Accepted: August 3, 2023
Published: August 16, 2023

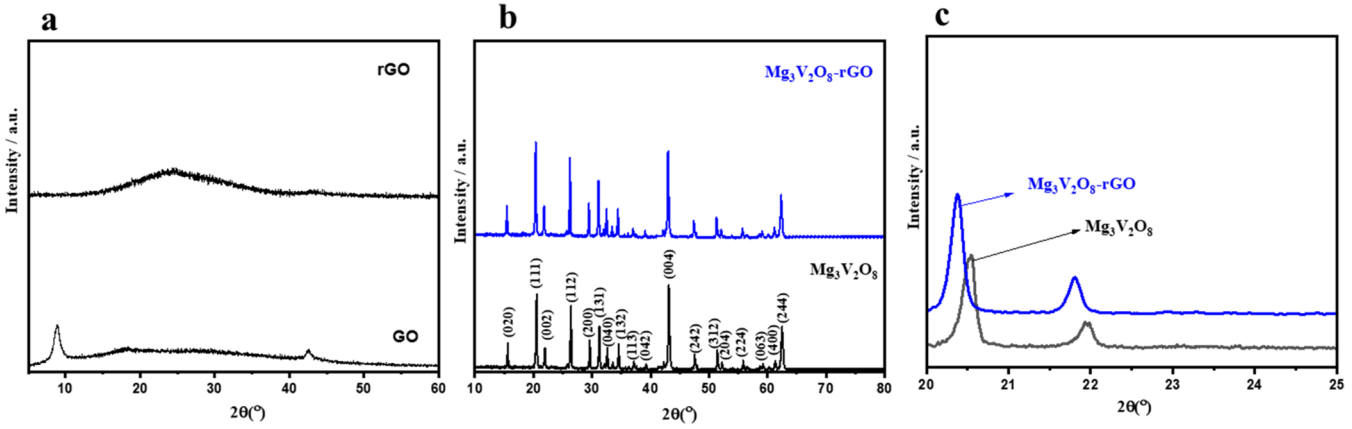

Figure 1. (a) PXRD patterns of GO and rGO (a) and $Mg_3V_2O_8$ and $Mg_3V_2O_8$-rGO composites (b). (c) Enlarged view showing the change in the diffraction peak.

and characteristics, which make it a desirable and promising material for photocatalytic applications.[38] In a previous study, $Mg_3V_2O_8$ was adopted as a suitable active electrode material for water oxidation using visible-light irradiation.[38] Therefore, it is clear from the above reports that $Mg_3V_2O_8$ possesses a reasonable potential for photocatalytic applications.

Herein, our group has obtained a $Mg_3V_2O_8$-rGO composite via simple strategies and approaches. Furthermore, the photocatalytic behavior of the as-synthesized $Mg_3V_2O_8$-rGO composite was investigated toward the production of H_2 using a photocatalytic approach. So far, no report has been found on the use of $Mg_3V_2O_8$-rGO as a photocatalyst for H_2 production. For the first time, we propose the photocatalytic H_2 production activities of the $Mg_3V_2O_8$-rGO composite. $Mg_3V_2O_8$-rGO demonstrated good photocatalytic activities toward H_2 evolution under visible light.

2. EXPERIMENTAL SECTION

2.1. Chemicals and Reagents. In this study, magnesium nitrate hexahydrate was purchased from Merck. Ammonium vanadate (AV) was purchased from Merck. Graphene oxide (GO) was purchased from Sigma. 2-Methyl imidazole (MIM) was purchased from Alfa-Aesar.

2.2. Synthesis of rGO, $Mg_3V_2O_8$, and $Mg_3V_2O_8$-rGO. For the synthesis of rGO, 50 wt % GO was dispersed in 100 mL of deionized water (DI) and sonicated for 2 h. Further, this dispersion was transferred to a Teflon cup covered with a stainless steel autoclave and heated at 200 °C for 6 h. The obtained product was washed with DI water and ethanol and dried in an oven for 6 h at 60 °C. For the preparation of $Mg_3V_2O_8$, 0.55 mmol of magnesium nitrate hexahydrate (ACS reagent, 99%) was dissolved in 10 mL of DI using magnetic stirring at room temperature (RT) for 10 min. In another beaker, 0.35 mmol of AV (99.95% trace metals basis) was dissolved in 10 mL of DI water using magnetic stirring at room temperature (RT) for 10 min. Further, the AV solution was slowly added to the above-prepared magnesium nitrate hexahydrate solution. Further, an aqueous solution of MIM (4.0 mmol) was also added to the above reaction mixture and stirred for 30 min at RT. Finally, this reaction mixture was transferred to the Teflon cup, and this Teflon cup was kept in a stainless steel autoclave. The autoclave was heated at 180 °C for 24 h and the precipitate was collected by centrifugation and dried at 70 °C for 6 h, which was further calcinated for 3 h at 450 °C. The obtained product was found to be $Mg_3V_2O_8$.

For the preparation of $Mg_3V_2O_8$-rGO, the obtained $Mg_3V_2O_8$ was dispersed in 20 mL of DI water using ultrasonication for 20 min. Further, an aqueous dispersion of GO was added to the $Mg_3V_2O_8$ dispersion solution and transferred to a Teflon cup, which was covered with the stainless steel autoclave. This autoclave was heated at 200 °C for 6 h, and the obtained product was washed with DI water and ethanol and dried in an oven for 6 h at 70 °C. This product was found to be $Mg_3V_2O_8$-rGO.

2.3. H_2 Production Process. Airtight quartz tube has been used as a photocatalytic reactor system for photocatalytic H_2 evolution studies. Twenty milliliters of lactic acid was added to 100 mL of water and 250 mg of photocatalyst ($Mg_3V_2O_8$ or $Mg_3V_2O_8$-rGO) was added to the above-prepared lactic acid solution. Further, nitrogen gas (N_2) was purged into the above solution for 30−40 min to extract the dissolved gases in the prepared solution. A 300 W LED (visible-light source) with a wavelength of 420 nm has been used for H_2 evolution studies. The produced H_2 was studied by a gas chromatograph.

2.4. Apparatus. To characterize the physiochemical characteristics of the fabricated samples, various techniques such as scanning electron microscopy (SEM; Zeiss), powder X-ray diffraction (PXRD, Rigaku, Japan), energy-dispersive X-ray spectroscopy (EDX; Oxford), photoluminescence (PL) spectroscopy, X-ray photoelectron spectroscopy (XPS), and ultraviolet−visible (UV−vis) spectroscopy (Agilent Cary Instrument) have been used.

3. RESULTS AND DISCUSSION

3.1. Physiochemical Properties of $Mg_3V_2O_8$-rGO. The obtained PXRD patterns of the synthesized samples (GO, rGO, $Mg_3V_2O_8$, and $Mg_3V_2O_8$-rGO) are shown in Figure 1a,1b. The obtained PXRD of GO exhibits the existence of a well-defined diffraction peak at ∼9.8°, which confirms the presence of the (002) diffraction plane of GO (Figure 1a). On the other side, rGO exhibits a characteristic broad diffraction peak related to the (002) diffraction plane of rGO, which suggested the transformation of GO to rGO (Figure 1a). The PXRD pattern of the synthesized $Mg_3V_2O_8$ shows various strong diffraction peaks and authenticated presence of (020), (111), (002), (112), (200), (131), (040), (132), (113), (042), (004), (242), (312), (204), (224), (063), (400), and (224) diffraction planes (Figure 1b). The obtained PXRD pattern of $Mg_3V_2O_8$ was matched with the JCPDS number 37-0351 and confirmed its formation.[36]

https://doi.org/10.1021/acsomega.3c04476
ACS Omega 2023, 8, 31493−31499

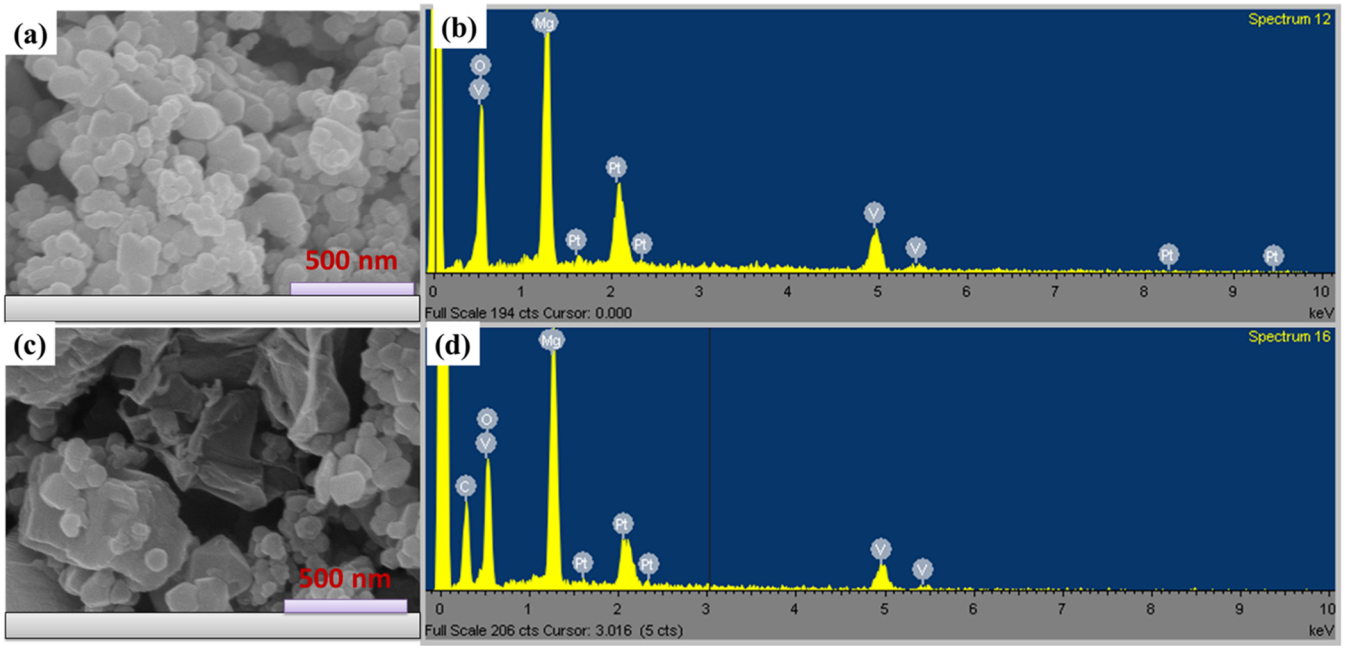

Figure 2. SEM images of $Mg_3V_2O_8$ (a) and $Mg_3V_2O_8$-rGO (c). EDX spectrum of $Mg_3V_2O_8$ (b) and the $Mg_3V_2O_8$-rGO composite (d).

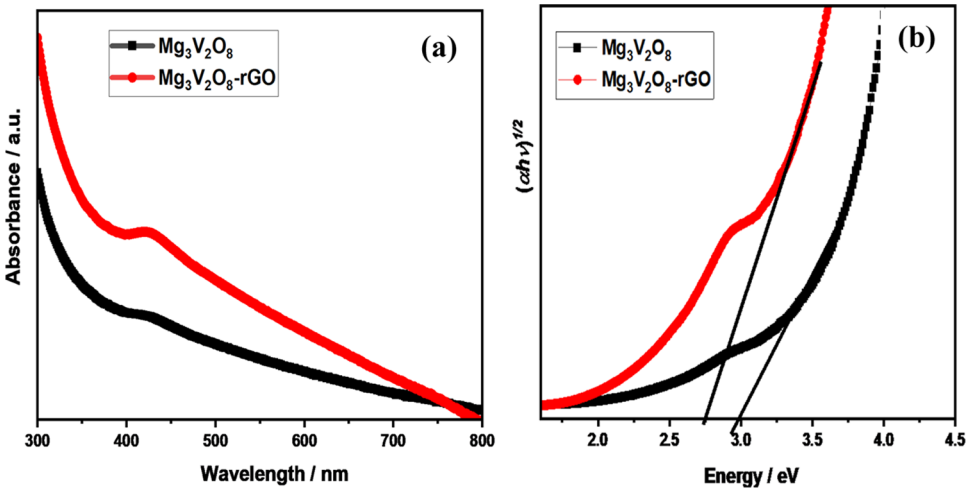

Figure 3. UV−vis absorption spectra of $Mg_3V_2O_8$ (black) and $Mg_3V_2O_8$-rGO (red) composite (a). Tauc plot of $Mg_3V_2O_8$ (black) and $Mg_3V_2O_8$-rGO (red) composite (b).

The PXRD pattern of the synthesized $Mg_3V_2O_8$-rGO is also displayed in Figure 1b. The PXRD pattern of $Mg_3V_2O_8$-rGO shows the presence of (020), (111), (002), (112), (200), (131), (040), (132), (113), (042), (004), (242), (312), (204), (224), (063), (400), and (224) diffraction planes of $Mg_3V_2O_8$. The presence of rGO could not be observed by PXRD analysis, which may be due to the amorphous nature or low content of rGO in the $Mg_3V_2O_8$-rGO sample. However, the introduction of rGO to the $Mg_3V_2O_8$ material shifted the diffraction peak, as shown in Figure 1c (enlarged view of Figure 1b). The electronic properties of rGO may significantly affect the X-ray with $Mg_3V_2O_8$, which may have shifted the PXRD peak (Figure 1c).

The surface morphology and structural properties of $Mg_3V_2O_8$ and $Mg_3V_2O_8$-rGO samples were also studied by employing the SEM technique. Figure 2a shows an SEM image of the prepared $Mg_3V_2O_8$, indicating that $Mg_3V_2O_8$ nanoparticles are formed. The $Mg_3V_2O_8$ nanoparticles were interconnected and formed an agglomeration of $Mg_3V_2O_8$ nanoparticles. The obtained SEM image of $Mg_3V_2O_8$-rGO is depicted in Figure 2c. The observations show that $Mg_3V_2O_8$ is embedded in the rGO sheets (Figure 2c).

It confirms the presence of $Mg_3V_2O_8$ in the prepared $Mg_3V_2O_8$-rGO sample. Furthermore, we have also recorded the EDX spectrum of the prepared $Mg_3V_2O_8$ and $Mg_3V_2O_8$-rGO samples to further characterize and verify the elemental composition. Figure 2b shows the EDX spectrum of $Mg_3V_2O_8$ and indicated the presence of Mg, V, and O elements. This suggested that $Mg_3V_2O_8$ has been formed. The obtained EDX spectrum of $Mg_3V_2O_8$-rGO is shown in Figure 2d. The obtained EDX spectrum exhibits the presence of C, Mg, V, and O elements. This revealed the successful synthesis of $Mg_3V_2O_8$-rGO. There was no other impurity element detected in the EDX spectrum of $Mg_3V_2O_8$-rGO, which confirmed its good phase purity.

https://doi.org/10.1021/acsomega.3c04476
ACS Omega 2023, 8, 31493−31499

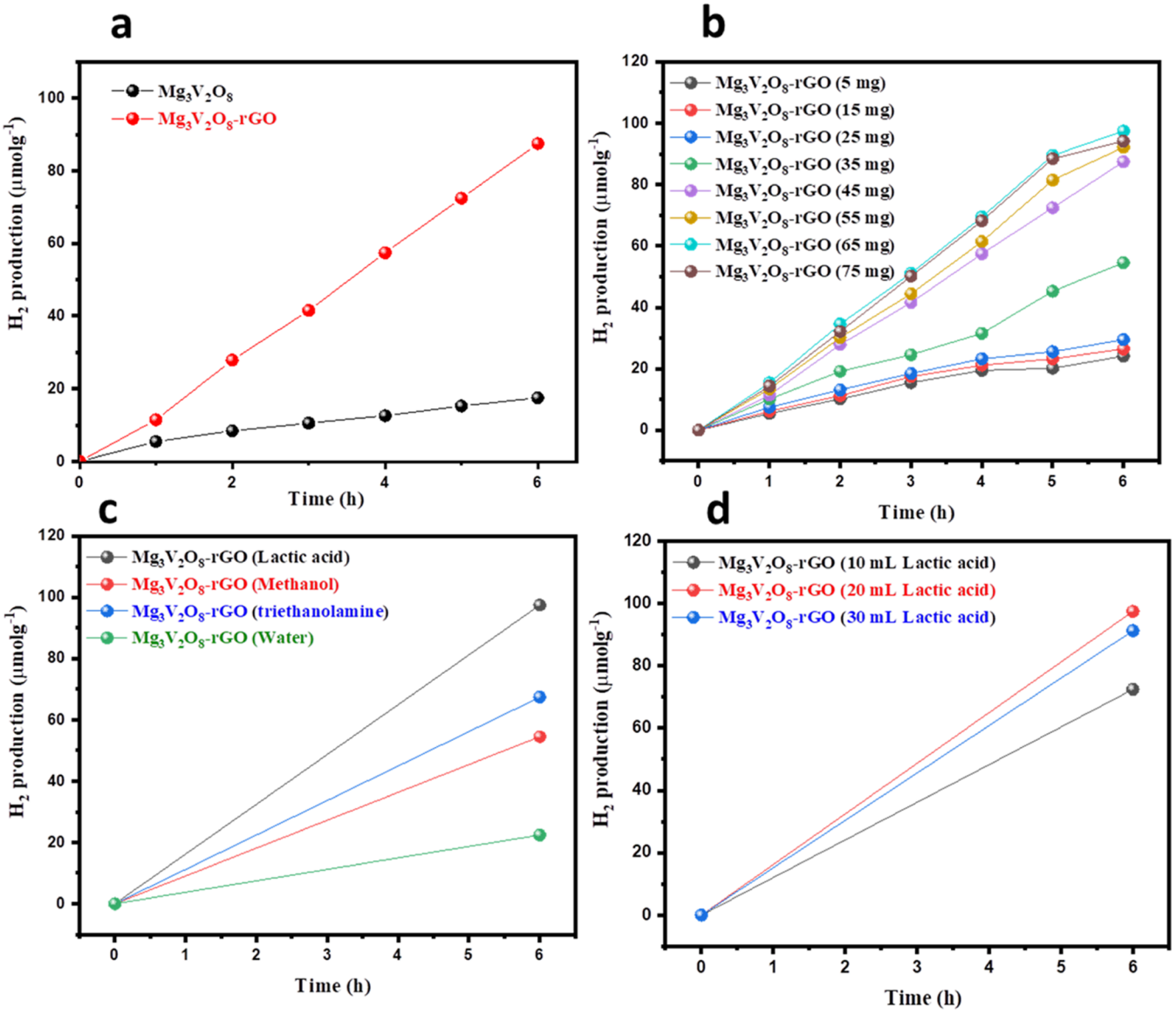

Figure 4. Photocatalytic H_2 production amount of $Mg_3V_2O_8$ and $Mg_3V_2O_8$-rGO catalysts (a). Photocatalytic H_2 production amount of the $Mg_3V_2O_8$-rGO catalyst with different doses (b). Photocatalytic H_2 production activity of $Mg_3V_2O_8$-rGO in different solvents (c). Photocatalytic H_2 production activity of $Mg_3V_2O_8$-rGO in different volumes of lactic acid (d).

The optical features such as the optical band gap of the prepared $Mg_3V_2O_8$ and $Mg_3V_2O_8$-rGO samples were determined by using UV−vis absorption spectroscopy. The obtained UV−vis spectra of $Mg_3V_2O_8$ and $Mg_3V_2O_8$-rGO are presented in Figure 3.

According to Figure 3a, a broad absorption band is observed around 423 nm. In the case of $Mg_3V_2O_8$-rGO, the absorption appeared at 429 nm. The band gaps of $Mg_3V_2O_8$ and $Mg_3V_2O_8$-rGO were calculated by utilizing the Tauc method. The optical study suggested that $Mg_3V_2O_8$ and $Mg_3V_2O_8$-rGO possess band gaps of 2.77 and 2.98 eV, respectively (Figure 3b).

Further, photoluminescence (PL) spectroscopy was also used to characterize the prepared $Mg_3V_2O_8$ and $Mg_3V_2O_8$-rGO samples. The PL spectra of the $Mg_3V_2O_8$ and $Mg_3V_2O_8$-rGO samples are shown in Figure S1. The PL spectrum of $Mg_3V_2O_8$ and $Mg_3V_2O_8$-rGO exhibited a PL peak between 550 to 600 nm. X-ray photoelectron spectroscopy (XPS) was also adopted to examine the elemental composition of the prepared $Mg_3V_2O_8$-rGO. The XPS survey spectrum of $Mg_3V_2O_8$-rGO is shown in Figure S2a. The survey spectrum confirmed the presence of Mg, V, O, and C elements, which indicated the formation of $Mg_3V_2O_8$-rGO. The high-resolution C 1s, Mg 1s, V 2p, and O 1s of $Mg_3V_2O_8$-rGO are shown in Figures S2b−e.[39] The C 1s scan revealed the presence of binding energies of 284.27 and 288.7 eV for graphitic carbon atoms and C═O groups, respectively. This indicated the presence of rGO in the prepared $Mg_3V_2O_8$-rGO sample.

The binding energy value of 1303.5 eV can be assigned to Mg 1s, as shown in Figure S2c. The binding energy value of 524.73 and 517.22 eV may be assigned to the presence of $2p_{1/2}$ and $2p_{3/2}$, respectively (Figure S2d). The O 1s scan of $Mg_3V_2O_8$-rGO exhibited binding energy values of 531.5 and 529.4 eV, which can be ascribed to the presence of Mg−O and V−O bonds, respectively (Figure S2e).[40] These excellent physiochemical and optical properties of $Mg_3V_2O_8$ and $Mg_3V_2O_8$-rGO suggested their potential for photocatalytic applications. Thus, we have adopted the use of $Mg_3V_2O_8$ and

https://doi.org/10.1021/acsomega.3c04476
ACS Omega 2023, 8, 31493−31499

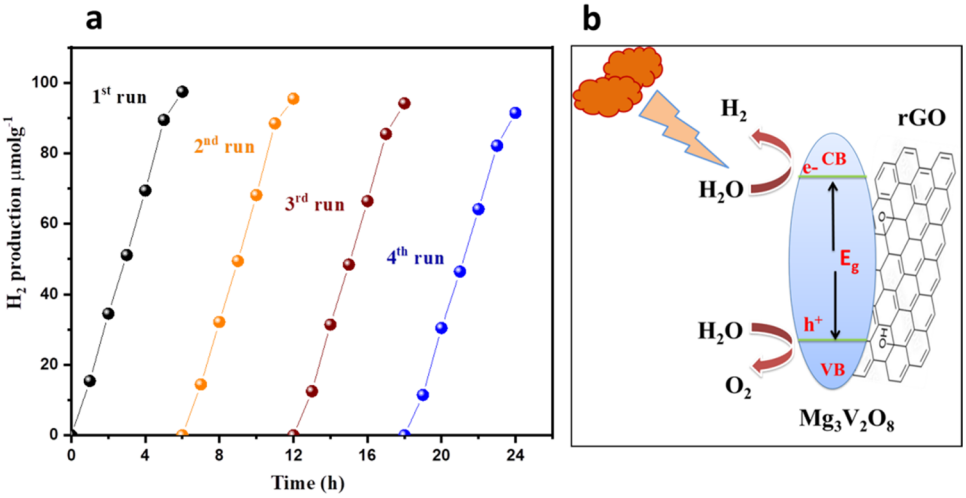

Figure 5. Photocatalytic H_2 production reusability study of the $Mg_3V_2O_8$-rGO catalyst (a). Probable mechanism of the $Mg_3V_2O_8$-rGO catalyst for H_2 production (b).

$Mg_3V_2O_8$-rGO as effective and efficient photocatalysts for H_2 evolution.

3.2. H_2 Production Activities of $Mg_3V_2O_8$ and $Mg_3V_2O_8$-rGO. The photocatalytic properties of the fabricated $Mg_3V_2O_8$ and $Mg_3V_2O_8$-rGO catalysts were evaluated in the presence of 20 mL of lactic acid in 100 mL of water. The H_2 evolution activities of $Mg_3V_2O_8$ and $Mg_3V_2O_8$-rGO were studied under visible-light irradiation. In this investigation, 25 mg of photocatalyst ($Mg_3V_2O_8$ or $Mg_3V_2O_8$-rGO) was used. Further, nitrogen (N_2) gas was passed in the solution prepared above for 30 min. The above solution was irradiated with LED light (xenon lamp) for different times (1, 2, 3, 4, 5, and 6 h). At a particular time interval, generated H_2 was collected by syringe and examined by a gas chromatograph. The obtained results are summarized in Figure 4a. The reasonable H_2 evolution of 17.54 μmol g^{-1} appeared for $Mg_3V_2O_8$ catalysts. However, enhanced H_2 production of 87.45 μmol g^{-1} has been obtained using the $Mg_3V_2O_8$-rGO catalyst as shown in Figure 4a. This excellent photocatalytic property of the $Mg_3V_2O_8$-rGO photocatalyst may be attributed to the presence of synergistic effects between rGO and $Mg_3V_2O_8$. The amounts of $Mg_3V_2O_8$ and $Mg_3V_2O_8$-rGO catalysts were also optimized in 20 mL of lactic acid. Different amounts (5, 15, 25, 35, 45, 55, 65, and 75 mg) of $Mg_3V_2O_8$ or $Mg_3V_2O_8$-rGO have been used for photocatalytic H_2 evolution studies. The obtained results are presented in Figure 4b. It can be observed from Figure 4b that the H_2 evolution amount increases with the increasing number of catalysts ($Mg_3V_2O_8$ or $Mg_3V_2O_8$-rGO) from 5 to 65 mg (Figure 4b). However, relatively lower H_2 was generated with 75 mg of photocatalyst, which suggested that 65 mg of photocatalyst is the optimized amount for the photocatalytic H_2 evolution process. Thus, we have used this optimized amount of 65 mg of catalyst for further photocatalytic studies. Subsequently, we have examined the photocatalytic properties of $Mg_3V_2O_8$ or $Mg_3V_2O_8$-rGO in various solvents (methanol, lactic acid, triethanolamine, and water). The obtained photocatalytic results are summarized in Figure 4c. It can be seen that $Mg_3V_2O_8$ or $Mg_3V_2O_8$-rGO possesses poor photocatalytic properties in pure water. However, relatively higher photocatalytic H_2 generation was observed for triethanolamine and methanol solvents. The highest amount of H_2 was generated for lactic acid using $Mg_3V_2O_8$ or $Mg_3V_2O_8$-rGO catalysts.

It can be observed that $Mg_3V_2O_8$-rGO has shown excellent improvements in photocatalytic H_2 evolution compared to $Mg_3V_2O_8$ (Figure 4c). We have also checked the photocatalytic properties of $Mg_3V_2O_8$ or $Mg_3V_2O_8$-rGO by varying the amount of lactic acid. Figure 4d shows the photocatalytic H_2 production activities of $Mg_3V_2O_8$ or $Mg_3V_2O_8$-rGO in the presence of different amounts (10, 20, and 30 mL) of lactic acid. The highest amount of H_2 was generated for 20 mL of lactic acid compared to 10 or 30 mL of lactic acid. The highest H_2 production of 72.45 and 97.45 μmol g^{-1} were observed for 20 mL of lactic acid using $Mg_3V_2O_8$ and $Mg_3V_2O_8$-rGO, respectively (Figure 4d). The obtained results are impressive for the $Mg_3V_2O_8$-rGO catalyst compared to $Mg_3V_2O_8$. The reusability of the photocatalysts is a challenging task and plays a vital role in large-scale H_2 production applications. We have studied the reusability study of the $Mg_3V_2O_8$-rGO catalyst for 20 mL of lactic acid. Figure 5a demonstrates the reusability study of the $Mg_3V_2O_8$-rGO catalyst. There was insignificant degradation in the performance of the $Mg_3V_2O_8$-rGO catalyst observed up to four cycles.

The probable mechanism for H_2 production using the $Mg_3V_2O_8$-rGO catalyst has been schematically presented in Figure 5b. The visible light irradiated over the $Mg_3V_2O_8$-rGO catalyst generated electron−hole pairs as shown in eq i[41,42]

$$Mg_3V_2O_8 - rGO \rightarrow Mg_3V_2O_8 - rGO \times (h^+_{VB} + e^-_{CB}) \quad \text{(i)}$$

$$Mg_3V_2O_8 - rGO*(h^+_{VB}) + H_2O \rightarrow H^+ + {}^{\bullet}OH \quad \text{(ii)}$$

$$Mg_3V_2O_8 - rGO*(e^-_{CB}-) + H^+ \rightarrow 1/2H_2 \quad \text{(iii)}$$

$${}^{\bullet}OH + \text{lactic acid} \rightarrow H_2O + CO_2 \quad \text{(iv)}$$

The generated e^- in $Mg_3V_2O_8$ may move toward the conduction band of rGO and can be trapped due to the resonance effect. Therefore, it can be assumed that the synergistic interactions between $Mg_3V_2O_8$ and rGO may assist the charge separation between the generated e^-−h^+ pairs. The remaining h^+ at the valence band interacts with the surrounding H_2O molecules to form the H^+ ions and reactive

https://doi.org/10.1021/acsomega.3c04476
ACS Omega 2023, 8, 31493−31499

hydroxyl radicals ($^{\bullet}OH$) as shown in eq ii. The H^+ ions can move to the conduction band and thereby interact with e^- on the rGO surface and result in the formation of H_2 as described in eq iii. The sacrificial reagent (lactic acid) can also interact with $^{\bullet}OH$ to form oxidized products and H^+ ions (eq iv), which can further reduce to H_2 gas on the surface of rGO. Therefore, the combined efforts of photocatalytic water splitting and the lactic acid reforming process work together to enhance H_2 production.

4. CONCLUSIONS

In this work, a new photocatalyst has been developed by merging the physiochemical properties of $Mg_3V_2O_8$ and rGO. Simple strategies have been adopted to fabricate $Mg_3V_2O_8$ and $Mg_3V_2O_8$-rGO. The photocatalytic properties of $Mg_3V_2O_8$-rGO were studied toward the evolution of H_2 using a photocatalytic approach. $Mg_3V_2O_8$-rGO showed an H_2 production amount of 97.45 μmol g^{-1} and an H_2 production rate of 16.24 μmol g^{-1} h^{-1}, which are relatively higher than that of the pristine $Mg_3V_2O_8$. $Mg_3V_2O_8$-rGO also demonstrated excellent reusability up to four cycles. This superior photocatalytic performance of $Mg_3V_2O_8$-rGO can be assigned to the presence of synergistic effects and improved charge-carrier transport properties. We proposed a low-cost and environmentally friendly photocatalyst for the H_2 evolution application.

ASSOCIATED CONTENT

Supporting Information

The Supporting Information is available free of charge at https://pubs.acs.org/doi/10.1021/acsomega.3c04476.

PL spectra of $Mg_3V_2O_8$ (black) and $Mg_3V_2O_8$-rGO (red) composite (Figure S1). XPS survey scan of the $Mg_3V_2O_8$-rGO (a) composite; high-resolution XPS C 1s (b), Mg 1s (c), V 2p (d), and O 1s (e) of the $Mg_3V_2O_8$-rGO composite (Figure S2) (PDF)

AUTHOR INFORMATION

Corresponding Authors

Fahad A. Alharthi − *Department of Chemistry, College of Science, King Saud University, Riyadh 11451, Kingdom of Saudi Arabia*; orcid.org/0000-0001-7513-9777; Phone: +966-507976713; Email: fharthi@ksu.edu.sa

Imran Hasan − *Department of Chemistry, College of Science, King Saud University, Riyadh 11451, Kingdom of Saudi Arabia*; orcid.org/0000-0002-5661-0655; Phone: +966-507976713; Email: iabdulateef@ksu.edu.sa

Authors

Adel El Marghany − *Department of Chemistry, College of Science, King Saud University, Riyadh 11451, Kingdom of Saudi Arabia*

Naaser A. Y. Abduh − *Department of Chemistry, College of Science, King Saud University, Riyadh 11451, Kingdom of Saudi Arabia*

Complete contact information is available at: https://pubs.acs.org/10.1021/acsomega.3c04476

Notes

The authors declare no competing financial interest.

ACKNOWLEDGMENTS

The authors extend their appreciation to the Deputyship for Research & Innovation, "Ministry of Education" in Saudi Arabia for funding this research work through the project number (IFKSUDR_E172).

REFERENCES

(1) Ahmad, K.; Khan, M. Q.; Khan, R. A.; Kim, H. Numerical Simulation and Fabrication of Pb-free Perovskite Solar Cells (FTO/TiO_2/$Cs_3Bi_2I_9$/spiro-MeOTAD/Au). *Opt. Mater.* **2022**, *128*, No. 112458.

(2) Ahmad, K.; Song, G.; Kim, H. Fabrication of Tungsten Oxide/Graphene Quantum Dot (WO_3@GQD) Thin Films on Indium Tin Oxide-Based Glass and Flexible Substrates for the Construction of Electrochromic Devices for Smart Window Applications. *ACS Sustainable Chem. Eng.* **2022**, *10* (36), 11948−11957.

(3) Ahmad, K.; Kim, H. Enhanced Stability of $MAPbI_3$ based Perovskite Solar Cells. *Mater. Lett.* **2022**, *318*, No. 132187.

(4) Dhabarde, N.; Selvaraj, J.; Yuda, A.; Kumar, A.; Subramanian, V. R. Review of Photocatalytic and Photo-electrocatalytic Reduction of CO_2 on Carbon Supported Films. *Int. J. Hydrogen Energy* **2022**, *47*, 30908−30936.

(5) Ahmad, K. *Bismuth Halide Perovskites for Photovoltaic Applications. In Bismuth—Fundamentals and Optoelectronic Applications*; IntechOpen: London, UK, 2020.

(6) Allured, B.; DelaCruz, S.; Darling, T.; Huda, M. N.; Subramanian, V. R. Enhancing the visible light absorbance of $Bi_2Ti_2O_7$ through Fe-substitution and its effects on photocatalytic hydrogen evolution. *Appl. Catal., B* **2014**, *144*, 261−268.

(7) Ragsdale, W.; Gupta, S.; Conard, K.; Delacruz, S.; Subramanian, V. R. Photocatalytic Activity of Fe-modified Bismuth Titanate Pyrochlores: Insights into its Stability, Photoelectrochemical, and Optical responses. *Appl. Catal., B* **2016**, *180*, 442−450.

(8) Khanal, V.; Ragsdale, W.; Gupta, S.; Subramanian, V. R. Insights into the Photoactivity of Iron Modified Bismuth Titanate (Fe_BTO) Nanoparticles. *Catal. Today* **2018**, *300*, 81−88.

(9) Mondal, A.; Prabhakaran, A.; Gupta, S.; Subramanian, V. R. Boosting Photocatalytic Activity Using Reduced Graphene Oxide (RGO)/Semiconductor Nanocomposites: Issues and Future Scope. *ACS Omega* **2021**, *6*, 8734−8743.

(10) Raza, W.; Ahmad, K. Visible Light-Driven Photocatalysts for Environmental Applications Based on Graphitic Carbon Nitride. In *Handbook of Nanomaterials and Nanocomposites for Energy and Environmental Applications*; Kharissova, O.; Martínez, L.; Kharisov, B., Eds.; Springer: Cham, 2020.

(11) Raza, W.; Ahmad, K.; Kim, H. Fabrication of Defective Graphene Oxide for Efficient Hydrogen Production and Enhanced 4-nitro-phenol Reduction. *Nanotechnology* **2021**, *32*, No. 495404.

(12) Ahmad, K.; Khan, M. Q.; Alsalme, A.; Kim, H. Sulfur-doped graphitic-carbon nitride (S@g-C_3N_4) as bi-functional catalysts for hydrazine sensing and hydrogen production applications. *Synth. Met.* **2022**, *288*, No. 117100.

(13) Tong, H.; Ouyang, S.; Bi, Y.; Umezawa, N.; Oshikiri, M.; Ye, J. Nano-photocatalytic Materials: Possibilities and Challenges. *Adv. Mater.* **2012**, *24*, 229−251.

(14) Fujishima, A.; Honda, K. Electrochemical Photolysis of Water at a Semiconductor Electrode. *Nature* **1972**, *238*, 37−38.

(15) Jiang, W. J.; Zhu, Y. F.; Zhu, G. X.; Zhang, Z. J.; Chen, X. J.; Yao, W. Q. Three-dimensional photocatalysts with a network structure. *J. Mater. Chem. A* **2017**, *5*, 5661−5679.

(16) Low, J.; Yu, J.; Jaroniec, M.; Wageh, S.; Al-Ghamdi, A. A. Heterojunction Photocatalysts. *Adv. Mater.* **2017**, *29*, No. 1601694.

(17) Sun, S.; Ren, D.; Yang, M.; Cui, J.; Yang, Q.; Liang, S. In-situ construction of direct Z-scheme sea-urchin-like ZnS/SnO_2 heterojunctions for boosted photocatalytic hydrogen production. *Int. J. Hydrogen Energy* **2022**, *47*, 9201−9208.

(18) Saldaña-Ramírez, A.; Alfaro Cruz, M. R.; Juárez-Ramírez, I.; Torres-Martínez, L. M. Influence of the power density and working

pressure in the magnetron co-sputtering deposition of ZnO−SnO_2 thin films and their effect in photocatalytic hydrogen production. *Opt. Mater.* **2020**, *110*, No. 110501.
(19) Yu-Cheng, C.; Yu-Wen, L. MoS_2@SnO_2 core-shell submicrospheres for high efficient visible-light photodegradation and photocatalytic hydrogen production. *Mater. Res. Bull.* **2020**, *129*, No. 110912.
(20) Li, B.; Wang, Y.; Zeng, Y.; Wang, R. Synthesis of CuO microsphere combined with g-C_3N_4 using Cu_2O as precursor for enhanced photocatalytic hydrogen evolution. *Mater. Lett.* **2016**, *178*, 308−311.
(21) Huang, S.; Bao, R.; Wang, J.; Yi, J.; Zhang, Z.; Liu, L.; Han, Y.; Li, Z.; Min, D.; Zhang, W.; Ge, Z.; Zhang, X. Synergistic effect of oxygen vacancy defects and TiO_2/WO_3 heterostructures in photocatalytic hydrogen production and dye degradation. *J. Alloys Compd.* **2023**, *961*, No. 170945.
(22) Dong, X.; Wang, H.; Li, X.; Fatehi, P.; Wang, S.; Wu, Q.; Liu, K.; Kong, F. In-situ sulfidation to fabricate NiSx modified g-C_3N_4/NiO composite for efficient photocatalytic hydrogen production under visible-light. *Appl. Surf. Sci.* **2023**, *610*, No. 155570.
(23) Chen, L.; Xie, X.; Su, T.; Ji, H.; Qin, Z. Co_3O_4/CdS p-n heterojunction for enhancing photocatalytic hydrogen production: Co-S bond as a bridge for electron transfer. *Appl. Surf. Sci.* **2021**, *567*, No. 150849.
(24) Wei, D.; Ding, Y.; Li, Z. Noble-metal-free Z-Scheme MoS_2−CdS/WO_3−MnO_2 nanocomposites for photocatalytic overall water splitting under visible light. *Int. J. Hydrogen Energy* **2020**, *45*, 17320−17328.
(25) Dhabarde, N.; Carrillo-Ceja, O.; Tian, S.; Xiong, G.; Raja, K.; Ravi Subramanian, V. Bismuth Vanadate Encapsulated with Reduced Graphene Oxide: A Nanocomposite for Optimized Photocatalytic Hydrogen Peroxide Generation. *J. Phys. Chem. C* **2021**, *125*, 23669−23679.
(26) Wang, D.; Tang, J.; Zou, Z.; Ye, J. Photophysical and Photocatalytic Properties of a New Series of Visible-Light-Driven Photocatalysts $M_3V_2O_8$ (M = Mg, Ni, Zn). *Chem. Mater.* **2005**, *17*, 5177.
(27) Butt, F. K.; Cao, C.; Ahmed, R.; Khan, W. S.; Cao, T.; Bidin, N.; Li, P.; Wan, Q.; Qu, X.; Tahir, M.; Idrees, F. Synthesis of novel ZnV_2O_4 spinel oxide nanosheets and their hydrogen storage properties. *CrystEngComm* **2014**, *16*, 894−899.
(28) Ma, H.; Zhang, S.; Ji, W.; Tao, Z.; Chen, J. a-CuV_2O_6 nanowires: hydrothermal synthesis and primary lithium battery application. *J. Am. Chem. Soc.* **2008**, *130*, 5361−5367.
(29) Xiao, L.; Zhao, Y.; Yin, J.; Zhang, L. Clewlike ZnV_2O_4 hollow spheres: nonaqueous sol−gel synthesis, formation mechanism, and lithium storage properties. *Chem. - Eur. J.* **2009**, *15*, 9442−9450.
(30) Shi, R.; Wang, Y.; Zhou, F.; Zhu, Y. $Zn_3V_2O_7(OH)_2(H_2O)_2$ and $Zn_3V_2O_8$ nanostructures: controlled fabrication and photocatalytic performance. *J. Mater. Chem.* **2011**, *21*, 6313−6320.
(31) Mondal, C.; Ganguly, M.; Sinha, A. K.; Pal, J.; Sahoo, R.; Pal, T. Robust cubooctahedron $Zn_3V_2O_8$ in gram quantity: a material for photocatalytic dye degradation in water. *CrystEngComm* **2013**, *15*, 6745−6751.
(32) Sambandam, B.; Soundharrajan, V.; Song, J.; Kim, S.; Jo, J.; Pham, D. T.; Kim, S.; Mathew, V.; Kim, J. $Zn_3V_2O_8$ porous morphology derived through a facile and green approach as an excellent anode for high-energy lithium ion batteries. *Chem. Eng. J.* **2017**, *328*, 454−463.
(33) Vijayakumar, S.; Lee, S. H.; Ryu, K. S. Synthesis of $Zn_3V_2O_8$ nanoplatelets for lithium-ion battery and supercapacitor applications. *RSC Adv.* **2015**, *5*, 91822−91828.
(34) Ye, J.; Zou, Z.; Arakaw, H.; Oshikiri, M.; Shimoda, M.; Matsushita, A.; Shishido, T. Correlation of crystal and electronic structures with photophysical properties of water splitting photocatalysts $InMO_4$ (M = V^{5+}, Nb^{5+}, Ta^{5+}). *J. Photochem. Photobiol., A* **2002**, *148*, 79−83.
(35) Kudo, A.; Omori, K.; Kato, H. A Novel Aqueous Process for Preparation of Crystal Form-Controlled and Highly Crystalline $BiVO_4$ Powder from Layered Vanadates at Room Temperature and Its Photocatalytic and Photophysical Properties. *J. Am. Chem. Soc.* **1999**, *121*, 11459−11467.
(36) Li, P.; Zhou, Y.; Tu, W.; Liu, Qi.; Yan, S.; Zou, Z. Direct Growth of $Fe_2V_4O_{13}$ Nanoribbons on a Stainless-Steel Mesh for Visible-Light Photoreduction of CO_2 into Renewable Hydrocarbon Fuel and Degradation of Gaseous Isopropyl Alcohol. *ChemPlusChem* **2013**, *78*, 274−278.
(37) Konta, R.; Kato, H.; Kobayashi, H.; Kudo, A. Photophysical properties and photocatalytic activities under visible light irradiation of silver vanadates. *Phys. Chem. Chem. Phys.* **2003**, *5*, 3061−3065.
(38) Mirsadeghi, S.; Ghoreishian, S. M.; Zandavar, H.; Behjatmanesh-Ardakani, R.; Naghian, E.; Ghoreishian, M.; Mehrani, A.; Abdolhoseinpoor, N.; Reza Ganjali, M.; Huh, Y. S.; Pourmortazavi, S. M. In-depth insight into the photocatalytic and electrocatalytic mechanisms of $Mg_3V_2O_8$@$Zn_3V_2O_8$@ZnO ternary heterostructure toward linezolid: Experimental and DFT studies. *J. Environ. Chem. Eng.* **2023**, *11*, No. 109106.
(39) Low, W. H.; Khiew, P. S.; Lim, S. S.; Siong, C. W.; Chia, C. H.; Ezeigwe, E. R. Facile synthesis of graphene-$Zn_3V_2O_8$ nanocomposite as a high performance electrode material for symmetric supercapacitor. *J. Alloys Compd.* **2019**, *784*, 847−858.
(40) Ma, X. F.; Li, H. Y.; Gao, D.; Ren, W.; Diao, J.; Xie, B.; Huang, G.; Wang, J.; Pan, F. $Mg_3V_2O_8$: A Promising Cathode Material for Aqueous Mg-ion Battery. In *Magnesium Technology*; Barela, S.; Leonard, A.; Maier, P.; Neelameggham, N. R.; Miller, V. M., Eds.; The Minerals, Metals & Materials Series; Springer: Cham, 2023.
(41) Kondarides, D. I.; Daskalaki, V. M.; Patsoura, A.; Verykios, X. E. Hydrogen Production by Photo-Induced Reforming of Biomass Components and Derivatives at Ambient Conditions. *Catal. Lett.* **2008**, *122*, 26−32.
(42) Wang, Y.; Liu, T.; Tian, W.; Zhang, Y.; Shan, P.; Chen, Y.; Wei, W.; Yuan, H.; Cui, H. Mechanism for Hydrogen Evolution from Water Splitting Based on a MoS_2/WSe_2 Heterojunction Photocatalyst: A First-Principle Study. *RSC Adv.* **2020**, *10*, 41127−41136.

https://doi.org/10.1021/acsomega.3c04476
ACS Omega 2023, 8, 31493−31499